Faraday Discussions

Cite this: Faraday Discuss., 2021, 227, 92



PAPER

View Article Online

Printable hexagonal boron nitride ionogels

Woo Jin Hyun,^a Lindsay E. Chaney,^a Julia R. Downing,^a Ana C. M. de Moraes^a and Mark C. Hersam (b) **abcd

Received 1st November 2019, Accepted 15th January 2020

DOI: 10.1039/c9fd00113a

Due to its excellent chemical/thermal stability and mechanical robustness, hexagonal boron nitride (hBN) is a promising solid matrix material for ionogels. While bulk hBN ionogels have been employed in macroscopic applications such as lithium-ion batteries, hBN ionogel inks that are compatible with high-resolution printing have not yet been realized. Here, we describe aerosol jet-printable ionogels using exfoliated hBN nanoplatelets as the solid matrix. The hBN nanoplatelets are produced from bulk hBN powders by liquid-phase exfoliation, allowing printable hBN ionogel inks to be formulated following the addition of an imidazolium ionic liquid and ethyl lactate. The resulting inks are reliably printed with variable patterns and controllable thicknesses by aerosol jet printing, resulting in hBN ionogels that possess high room-temperature ionic conductivities and storage moduli of >3 mS cm⁻¹ and >1 MPa, respectively. By integrating the hBN ionogel with printed semiconductors and electrical contacts, fullyprinted thin-film transistors with operating voltages below 1 V are demonstrated on polyimide films. These devices exhibit desirable electrical performance and robust mechanical tolerance against repeated bending cycles, thus confirming the suitability of hBN ionogels for printed and flexible electronics.

1. Introduction

Additive manufacturing based on high-resolution printing enables the production of electronic devices with minimal materials waste and low cost for a diverse set of applications including displays, distributed sensing, smart packaging, and energy management.¹⁻⁷ In addition, printing processes are compatible with roll-to-roll production schemes and flexible substrates, offering promise for high-throughput manufacturing of bendable and wearable devices. Among the range of additive manufacturing methods, aerosol jet printing has recently attracted considerable attention for printed electronics.⁸⁻¹² In this process (Fig. 1),

^aDepartment of Materials Science and Engineering, Northwestern University, Evanston, Illinois 60208, USA. E-mail: m-hersam@northwestern.edu

^bDepartment of Chemistry, Northwestern University, Evanston, Illinois 60208, USA

Department of Medicine, Northwestern University, Evanston, Illinois 60208, USA

^dDepartment of Electrical and Computer Engineering, Northwestern University, Evanston, Illinois 60208, USA

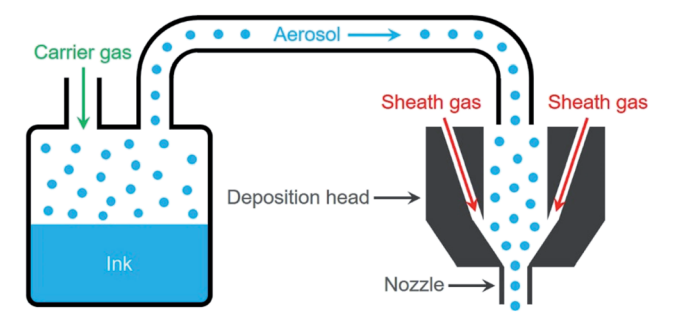


Fig. 1 Schematic of aerosol jet printing. The carrier gas flow delivers the aerosolized ink to the deposition head, and the sheath gas flow focuses the aerosol stream to achieve welldefined patterning.

a functional ink is aerosolized by an ultrasonic or pneumatic atomizer, and the aerosol droplets are delivered to the deposition head by a carrier gas flow. When the aerosol droplets pass through the nozzle of the deposition head, a coaxial sheath gas aerodynamically focuses the aerosol stream, enabling high-resolution deposition with minimal risk of nozzle clogging. Aerosol jet printing has the additional advantage of relaxed rheological constraints on ink design, including compatibility with a wide range of ink viscosities (1-1000 MPa s). Furthermore, aerosol jet printing facilitates the deposition of functional materials on nonplanar surfaces because the nozzle can be placed with a long standoff distance (1-5 mm) from the substrate. Due to these compelling advantages, significant research efforts have sought to develop inks and explore printed electronics applications for aerosol jet printing.13-17

Ionogels are solid-state electrolytes based on ionic liquids and gelling solid matrices, which have been employed for a variety of applications including transistors, supercapacitors, batteries, and neuromorphic computing devices. 18-22 Ionic liquids offer several desirable features as electrolytes including nonflammability, negligible vapor pressure, and high thermal and electrochemical stability. Moreover, combining ionic liquids with a gelling solid matrix leads to a solid-state electrolyte that is mechanically robust and flexible with minimal leakage problems, as is needed for flexible electronics. Recently, hexagonal boron nitride (hBN) nanoplatelets have been introduced as a promising solid matrix for ionogels.23 As a solid matrix material, hBN possesses several beneficial attributes such as electrically insulating character, chemical inertness, thermal stability, and mechanical robustness. Furthermore, compared to conventional bulk hBN microparticles, the smaller particle size of hBN nanoplatelets enables significant enhancement of ionogel mechanical strength without compromising ionic conductivity.23 While these initial results are promising, current hBN ionogel formulations are not compatible with the high-resolution and high-throughput additive manufacturing methods that are used for printed electronics.

Here, we report the development of aerosol jet-printable ionogels based on exfoliated hBN nanoplatelets and the ionic liquid 1-ethyl-3-methylimidazolium bis(trifluoromethylsulfonyl)imide (EMIM-TFSI). The hBN nanoplatelets are scalably solution-exfoliated from bulk hBN and then mixed with EMIM-TFSI and ethyl lactate to formulate printable inks. The resulting printable hBN ionogels exhibit high ionic conductivities and mechanical strengths (*i.e.*, storage moduli) of >3 mS cm⁻¹ and >1 MPa, respectively, at 25 °C. Moreover, reliable printing is demonstrated using a standard aerosol jet printer and polyimide substrates. Finally, fully-printed thin-film transistors (TFTs) with the hBN ionogel as the dielectric on polyimide substrates show exemplary transfer and output characteristics in addition to excellent mechanical tolerance to bending.

2. Results and discussion

Fig. 2a and b show a photograph and a scanning electron microscopy image, respectively, of the exfoliated hBN nanoplatelets that are used in the formulation of the printable hBN ionogels. For the exfoliation of hBN nanoplatelets, bulk hBN microparticles were shear-mixed in ethanol with ethyl cellulose (EC) acting as the dispersing agent.24,25 The exfoliated hBN nanoplatelets and EC were separated from the shear-mixed dispersion by centrifuge-assisted sedimentation and flocculation. The collected hBN/EC solids were then heated at 400 °C for 3 h in air to decompose the EC stabilizer. This annealing process volatilizes most of the EC, but also leaves behind a thin amorphous carbon coating on the surface of the exfoliated hBN, which contributes to enhanced interactions between the hBN nanoplatelets and ionic liquids for stronger solidification of ionogels.23 Importantly for dielectric applications, the amorphous carbon coating is electrically insulating and thus does not cause unwanted leakage currents.23 To formulate a printable hBN ionogel ink (Fig. 2c), the exfoliated and annealed hBN nanoplatelets were mixed with EMIM-TFSI and ethyl lactate. The ratio between the hBN nanoplatelets and ionic liquid was 1:2 by weight to achieve 33% hBN solid loading of the ionogel (i.e., hBN and ionic liquid), and the concentration of the ionogel in ethyl lactate was 120 mg mL^{-1} .

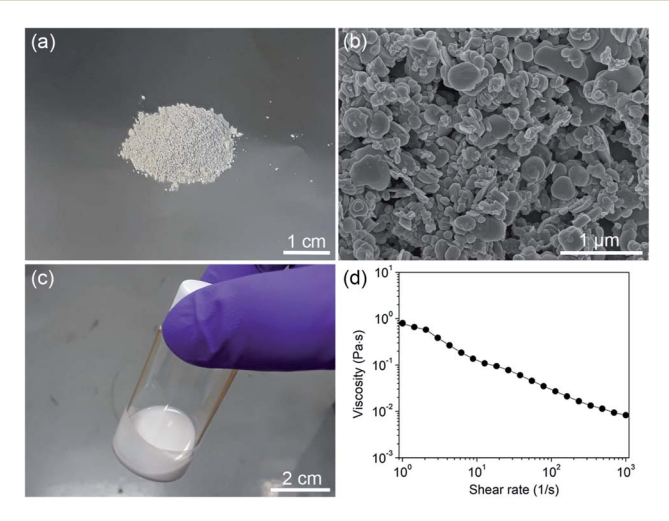


Fig. 2 (a) Photograph and (b) scanning electron microscopy image of exfoliated hexagonal boron nitride (hBN) nanoplatelets. (c) Photograph of a vial of the ionogel ink prepared with the hBN nanoplatelets. (d) Viscosity of the hBN ionogel ink as a function of shear rate at 25 °C.

In general, inks for aerosol jet printing are designed with the addition of a lowvolatility co-solvent (≤10%), such as terpineol or 1,8-octanedithiol. 26,27 Without the low-volatility co-solvent, aerosol droplets quickly lose solvent during transport from the ink container to the deposition head by the carrier gas flow, leading to poor morphology of the printed features. In contrast, the hBN ionogel ink only required a single solvent since the nonvolatile ionic liquid eliminates the need for an additional low-volatility co-solvent for effective printability. Fig. 2d shows the viscosity of the prepared hBN ionogel ink as a function of shear rate at 25 °C. The ink viscosity decreases as the shear rate increases, which can be attributed to the disruption of the interactions between the hBN nanoplatelets and the ionic liquid with increasing shear stress.²⁸ This shear thinning behavior is favorable for aerosol jet printing with an ultrasonic atomizer because inks experience high shear rates when generating aerosol droplets from a bulk liquid by ultrasonication.29 Hence, inks with shear thinning behavior require lower ultrasonic power for atomization, compared to Newtonian inks with a similar viscosity at low shear rates.

The mechanical properties and ionic conductivity of the printable hBN ionogel were characterized after evaporating ethyl lactate at a temperature (160 °C) that is higher than the boiling point (154 °C) of the solvent. As shown in Fig. 3a, the hBN ionogel (33% hBN solid loading) at 25 $^{\circ}$ C exhibits a storage modulus (G') higher than its loss modulus (G'') over the entire measured frequency range, revealing the reliable solid-like behavior of the hBN ionogel. This solid-like behavior (G' >G'') persists at temperatures in excess of 60 °C due to the strong solidification of

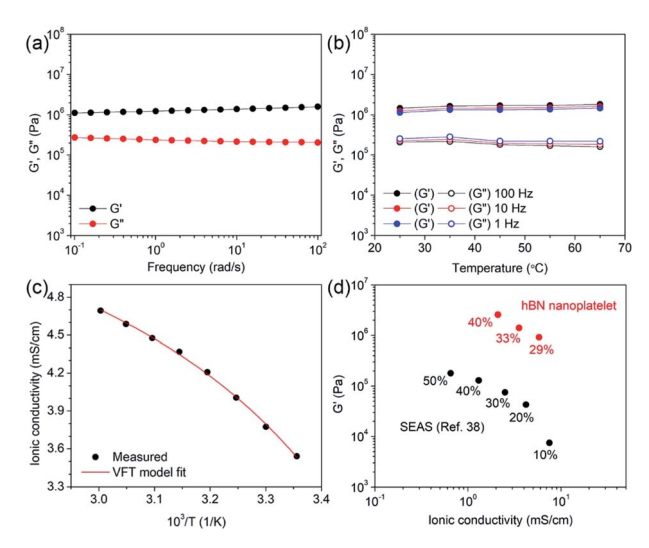


Fig. 3 (a) Storage (G') and loss (G'') moduli of the printable hBN ionogel (33% hBN solid loading) as a function of frequency at 25 $^{\circ}$ C. (b) G' and G'' of the hBN ionogel at various temperatures. (c) Temperature dependence of the ionic conductivity of the hBN ionogel (33% hBN solid loading). The black data points are the measured ionic conductivity values, and the red curve is a Vogel-Fulcher-Tammann (VFT) model fit. (d) G' and ionic conductivity of the hBN ionogels with various hBN solid loadings, and their comparison to previously reported ionogels (ref. 38) based on a triblock copolymer, poly(styrene-b-ethyl acrylate-b-styrene) (SEAS).

the hBN ionogel, as shown in Fig. 3b. In addition, the ionic conductivity of the hBN ionogel (33% hBN solid loading) is 3.4 ± 0.4 mS cm⁻¹ at 25 °C, and increases (Fig. 3c) with temperature in agreement with the Vogel–Fulcher–Tammann (VFT) model that correlates the ion conduction behavior with free volume and configurational entropy.^{30,31} The VFT model is expressed as:

$$\sigma = \sigma_0 \exp\left(-\frac{B}{T - T_0}\right)$$

where σ_0 , B, and T_0 are the pre-exponential factor equivalent to the ionic conductivity at infinite temperature, the pseudoactivation energy term related to the entropic barrier to ion motion, and the ideal glass transition temperature at which the free volume disappears, respectively. The parameters used for the VFT model curve (solid line in Fig. 3c) are 6.3 mS cm⁻¹, 20 K, and 263 K for σ_0 , B, and T_0 , respectively, resulting in a fit to the experimental data (data points in Fig. 3c) with a coefficient of determination (R^2) higher than 0.99.

Fig. 3d shows the mechanical strength (G') and ionic conductivity of the printable hBN ionogels for different hBN solid loadings. The printable hBN ionogels present a tradeoff between the mechanical strength and ionic conductivity as the hBN solid loading is varied. This tradeoff is typical for ionogels because increased solid loading enhances mechanical support but impedes ion motion.³²⁻³⁴ Moreover, Fig. 3d compares the mechanical strength and ionic conductivity of the printable hBN ionogels to previously reported printable ionogels based on triblock copolymer solid matrices. Printable ionogels based on triblock copolymers have been extensively developed due to their high ionic conductivity and printability, 35-37 although they typically suffer from poor mechanical strength. To address this issue, Tang et al. reported enhanced mechanical strength and ionic conductivity of printable ionogels based on poly(styrene-b-ethyl acrylate-b-styrene) (SEAS) and EMIM-TFSI ionic liquid by engineering the midblock chain of the triblock copolymer.³⁸ However, Fig. 3d shows that the printable hBN ionogels outperform even the SEAS-based ionogels, suggesting that the exfoliated hBN nanoplatelets are a promising solid matrix to concurrently achieve high mechanical strength and ionic conductivity.

To explore printability, the hBN ionogel ink (33% hBN solid loading) was printed using a commercially available aerosol jet printer with a nozzle size of 300 μm in diameter. The printing was performed on polyimide films without any surface pretreatment, and the substrate temperature was maintained at 60 °C during printing to promote ink drying. Fig. 4a displays an optical microscopy image of the printed hBN ionogel after 1 printing pass, showing a line width of \sim 280 µm and effective wetting on the polyimide substrate. As the number of printing passes increases (Fig. 4b-d), it is evident that the printed hBN ionogel layer increases in thickness, while the line width remains relatively constant, indicating minimal spreading of the hBN ionogel with a progressive number of printing passes. Similarly, Fig. 4e shows surface profiles of the printed hBN ionogels with different printing passes, which were taken along the dotted line in Fig. 4a by a laser confocal microscope. The surface profiles reveal convex crosssections of the hBN ionogels with a densely-deposited core region. As shown in Fig. 4f, the average thickness is linearly proportional to the number of printing passes, implying that the hBN ionogels are deposited homogeneously for each printing pass. In addition to the line features, a 1 mm \times 1 mm square pattern of

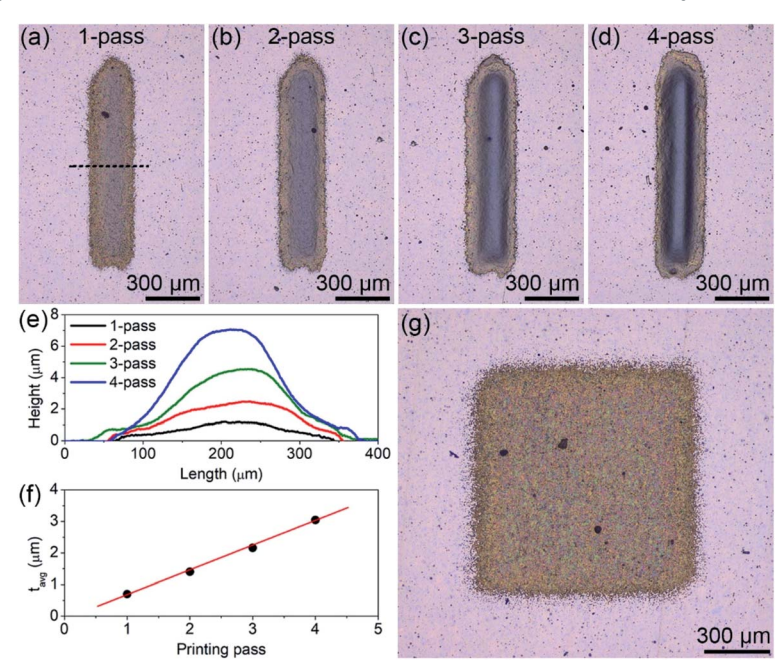


Fig. 4 Optical microscopy images of printed hBN ionogels with (a) 1, (b) 2, (c) 3, and (d) 4 printing passes on a polyimide film. (e) Cross-sectional profiles of the printed hBN ionogels as a function of the number of printing passes, taken along the dotted line in (a). (f) Average thickness (t_{avg}) of the printed hBN ionogels as a function of the number of printing passes. (g) Optical microscopy image of a printed hBN ionogel with a 1 mm imes 1 mm square pattern on a polyimide film.

the hBN ionogel was printed by successively depositing 1 mm long lines with a pitch of 50 μm. Fig. 4g shows an optical microscopy image of the deposited square pattern with minimal thickness variation, thus revealing uniform hBN ionogel printing over large areas.

To demonstrate the utility of the hBN ionogels in printed electronics, fullyprinted thin-film transistors (TFTs) using the hBN ionogel as the dielectric were fabricated on flexible substrates by aerosol jet printing, as shown in Fig. 5a. Ionogels are a favorable dielectric for flexible printed TFTs because the electrolytes offer high tolerance to thickness variations and desirable mechanical flexibility without leakage issues. Moreover, the high double-layer capacitance of ionogel electrolytes enables low-voltage operation for low-power and portable devices. To fabricate the TFTs (Fig. 5b), graphene was first deposited on polyimide films for the source and drain electrodes with a channel width and length of 700 μm and 70 μm, respectively. Poly(3-hexylthiophene) (P3HT) was then printed to form the semiconducting channel, and the hBN ionogel dielectric was deposited semiconducting channel. Finally, the poly(3,4ethylenedioxythiophene):poly(styrene sulfonate) (PEDOT:PSS) was printed onto the hBN ionogel dielectric as the gate electrode to complete the devices. The entire device fabrication and subsequent characterization were executed in ambient conditions, and the fabricated devices were annealed at 160 °C preceding electrical measurements to remove sequestered solvent.

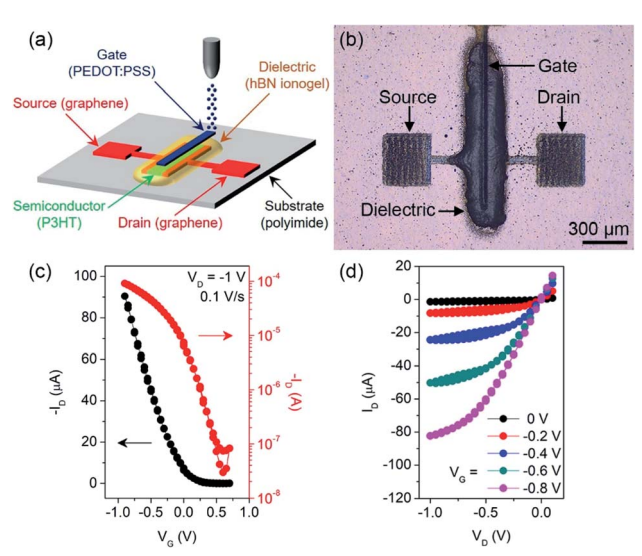


Fig. 5 (a) Schematic and (b) optical microscopy image of a fully-printed thin-film transistor (TFT) with the hBN ionogel dielectric on a polyimide film. (c) Representative transfer and (d) output characteristics for the printed TFT. I_D , V_D , and V_G denote drain current, drain voltage, and gate voltage, respectively. The TFT channel width and length were 700 and 70 μ m, respectively. The voltage sweep rate and V_D for the transfer curves were 0.1 V s⁻¹ and -1 V, respectively.

Fig. 5c shows a representative transfer characteristic of the fabricated TFTs at a sweep rate of 100 mV s⁻¹ and a drain voltage $(V_{\rm D})$ of -1 V. In the TFTs with the hBN ionogel dielectric, the drain current $(I_{\rm D})$ is low at positive gate voltage $(V_{\rm G})$ because the p-type semiconducting channel is depleted. However, $I_{\rm D}$ increases at negative $V_{\rm G}$ since anions in the ionogel dielectric are driven into the polymer semiconductor and compensate induced charge carriers in the TFT channel. This electrolytic gating enables the devices to operate with small $V_{\rm G}$ (less than 1 V), and the negligible hysteresis between forward and backward sweeps can be attributed to the fast response of the ions in the hBN ionogel dielectric to $V_{\rm G}$. Furthermore, the output curves (Fig. 5d) obtained at various $V_{\rm G}$ display the expected $I_{\rm D}$ modulation with linear and saturation regimes at low and high $V_{\rm D}$, respectively, demonstrating well-behaved operation of the fully-printed TFTs with the hBN ionogel dielectric.

The charge carrier mobility (μ) and the threshold voltage $(V_{\rm th})$ of the fabricated TFTs were calculated by fitting plots (Fig. 6a) of the square-root drain current $(I_{\rm D}^{-1/2})$ as a function of $V_{\rm G}$, according to the standard saturation regime relation:

$$I_{\mathrm{D}} = \mu C_{\mathrm{i}} \frac{W}{2L} (V_{\mathrm{G}} - V_{\mathrm{th}})^2$$

where C_i is the specific capacitance of the ionogel dielectric, W is the width (700 μ m) of the semiconducting channel, and L is the length (70 μ m) of the semiconducting channel. C_i was estimated to be 108 μ F cm⁻² by displacement current measurements,^{39,40} in which the gate current (I_G) was measured with source and drain contacts grounded at different sweep rates. Fig. 6b displays I_G – V_G

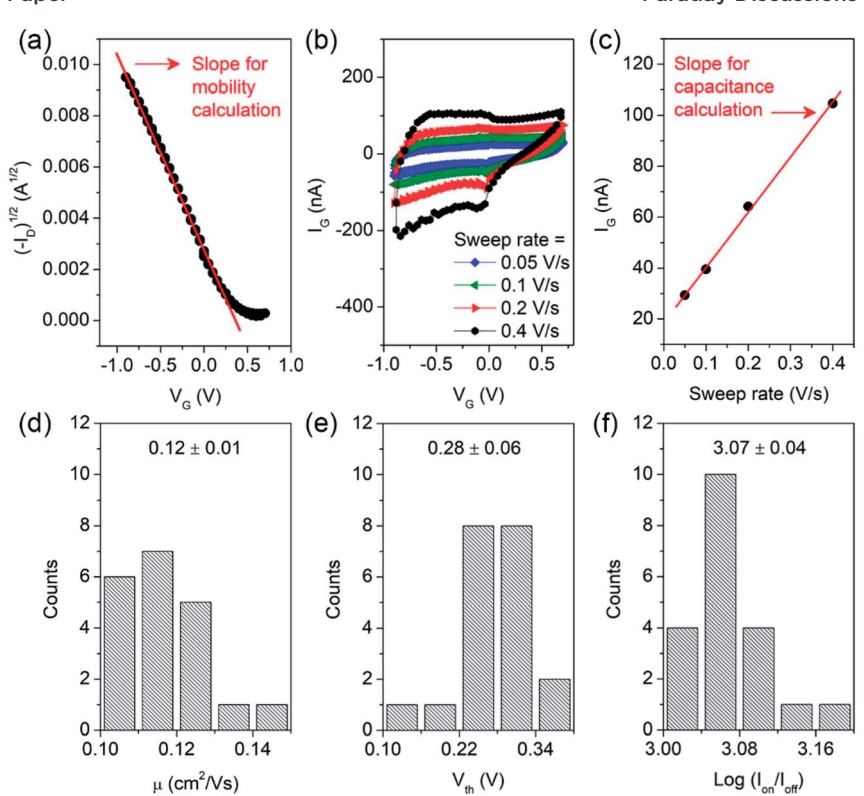


Fig. 6 (a) Representative $I_D^{1/2} - V_G$ characteristic for the printed TFTs. (b) $I_G - V_G$ characteristics measured at various sweep rates. I_G indicates gate current measured with source and drain contacts grounded. (c) Plot of I_G as a function of the sweep rate at V_G of -0.2 V. Histograms of (d) charge carrier mobility (μ), (e) threshold voltage (V_{th}), and (f) on/off-current ratio (I_{cn}/I_{off}) for 20 devices.

characteristics of a representative device at sweep rates between 0.05 V s⁻¹ and 0.4 V s⁻¹, and Fig. 6c shows the plot of $I_{\rm G}$ as a function of the sweep rate at $V_{\rm G}$ of -0.2 V for the capacitance calculation. Twenty TFTs were fabricated to evaluate statistical distributions of the device metrics. All of the devices were functional with μ (Fig. 6d), $V_{\rm th}$ (Fig. 6e), and on/off-current ratio ($I_{\rm on}/I_{\rm off}$, Fig. 6f) of the 20 devices measured to be 0.12 ± 0.01 cm² V⁻¹ s⁻¹, 0.28 ± 0.06 V, and 103.07 ± 0.04 , respectively. This excellent fabrication yield and minimal variation in the device metrics confirms the high reliability of the printable hBN ionogel for TFT-based printed electronics.

The deformable nature of the ionogel dielectric also enables mechanically flexible applications (Fig. 7a). To evaluate the mechanical stability of the flexible devices with the hBN ionogel dielectric, a bending test was performed with a bending radius (r) of 14 mm (Fig. 7b), corresponding to a tensile strain (d/2r) of 0.2% based on the substrate thickness (d) of 50 μ m. Fig. 7c shows the changes in the device metrics (μ and $V_{\rm th}$) during the bending test. Following 1000 bending cycles, μ was reduced by less than 3% (100% $-\mu/\mu_0$) and $V_{\rm th}$ was shifted by only \sim 0.05 V ($V_{\rm th}-V_{\rm th,0}$) from the initial values (μ_0 and $V_{\rm th,0}$). These minor changes in

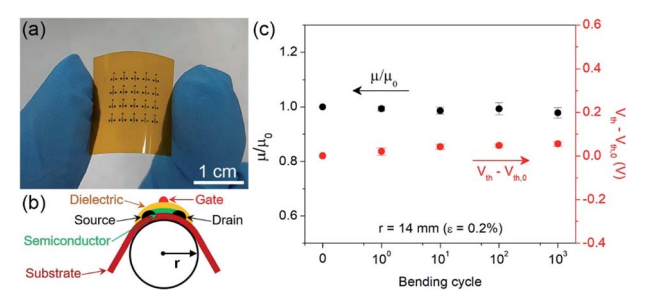


Fig. 7 (a) Photograph of a 4 \times 5 array of fully-printed TFTs on a polyimide film. (b) Schematic of the bending test for the printed TFTs. (c) Relative mobility (μ/μ_0) and threshold voltage change ($V_{\rm th}-V_{\rm th,0}$) after repeated bending cycles. The bending radius (r) was 14 mm, corresponding to a tensile strain (ε) of 0.2%.

the device performance after repeated bending cycles indicate the desirable mechanical resilience of the hBN ionogel dielectric for flexible electronics.

3. Conclusions

In summary, we have developed aerosol jet-printable ionogels employing exfoliated hBN nanoplatelets as the solid matrix. The hBN nanoplatelets were obtained from bulk hBN by scalable solution exfoliation, and the printable hBN ionogel inks were formulated by mixing the exfoliated hBN nanoplatelets, EMIM-TFSI, and ethyl lactate. The printable hBN ionogels show high ionic conductivities and mechanical strengths (*i.e.*, storage moduli) of >3 mS cm⁻¹ and >1 MPa (with 33% hBN solid loading at 25 °C), respectively. Furthermore, the hBN ionogels were aerosol jet-printed with variable patterns and controllable thicknesses, demonstrating well-behaved printability. Employing the hBN ionogel as a dielectric, fully-printed TFTs were also constructed on polyimide films with high uniformity, desirable transfer and output characteristics, and durable operation following repeated mechanical bending. Overall, this work establishes printable hBN ionogels as a robust and reliable dielectric material for low-voltage flexible and printed electronics.

4. Experimental details

Preparation of hBN ionogel inks

To exfoliate hBN nanoplatelets, a dispersion of bulk hBN (\sim 1 µm, Sigma-Aldrich), ethyl cellulose (4 cP viscosity grade, Sigma-Aldrich), and ethanol in a weight ratio of 10:1:52 was shear-mixed for 2 h at 10 230 rpm, using a rotor/stator mixer (L5M-A, Silverson) with a square hole screen. After centrifugation (J26-XPI, Beckman Coulter) of the shear-mixed dispersion at 4000 rpm for 20 min to remove large particles, the supernatant was collected and mixed with an aqueous solution of 40 mg mL $^{-1}$ sodium chloride in a 16:9 weight ratio to flocculate exfoliated hBN nanoplatelets and EC. After centrifuging the mixture at 7500 rpm for 6 min, the sediment containing exfoliated hBN nanoplatelets and EC was collected and washed with deionized water to remove residual sodium chloride, dried with an infrared lamp, and ground with a mortar and pestle to yield a fine

powder. The hBN/EC powder was then annealed at 400 °C for 3 h in air to decompose EC. To prepare the printable hBN ionogel ink, the hBN nanoplatelets were mixed with EMIM-TFSI and ethyl lactate by bath sonication for 6 h. The ratio of the hBN nanoplatelets and ionic liquid was 1 : 2 by weight for 33% hBN solid loading of the ionogel (hBN and ionic liquid), and the concentration of the ionogel in ethyl lactate was 120 mg mL $^{-1}$. The hBN ionogel ink was printed using a commercially available aerosol jet printer (Aerosol Jet 200, Optomec) with a 300 μ m diameter nozzle. The flow rates of the carrier gas and sheath gas were 15 sccm and 20 sccm, respectively, and the printing was performed with the substrate temperature maintained at 60 °C.

Fabrication of fully-printed TFTs

To prepare the graphene ink for the source and drain electrodes, graphene nanoplatelets were obtained by solution exfoliation of graphite flakes (Sigma-Aldrich).41,42 In particular, a dispersion of graphite flakes, EC, and ethanol in a 30:1:20 weight ratio was shear-mixed for 23 h using an inline mixer (200L, Silverson) equipped with a square hole screen. The shear-mixed dispersion was then centrifuged at 6500 rpm for 30 min to crash out unexfoliated graphite, after which the supernatant containing exfoliated graphene and EC was collected and flocculated with an aqueous solution of 40 mg mL^{-1} sodium chloride in a 16 : 9 weight ratio. After centrifuging the mixture at 7000 rpm for 7 min, the sediments containing graphene and EC were collected from the bottles and washed with deionized water to remove residual sodium chloride, dried with an infrared lamp, and ground with a mortar and pestle to yield a fine powder. The printable graphene ink was obtained by dispersing the graphene/EC (1:1 by weight) powder in a solvent system of ethyl lactate and terpineol (9: 1 by volume) at a concentration of 30 mg mL⁻¹ by bath sonication for 6 h. The graphene ink was printed on polyimide with a substrate temperature of 60 °C, and the printed graphene electrodes were further annealed at 300 °C for 30 min in air to decompose EC and thereby improve the electrical conductivity. Following the deposition of the source and drain electrodes, the semiconductor channel, hBN ionogel dielectric, and gate electrode were deposited sequentially by aerosol jet printing. The semiconductor channel was printed with an ink of P3HT (molecular weight: 50-100 K, Sigma-Aldrich) dissolved in a solvent system of chloroform/terpineol (9:1 by volume) at a concentration of 1 mg mL⁻¹. The gate electrode was printed with a conductive ink containing PEDOT:PSS (Clevios PH1000, Heraeus) and ethylene glycol (9:1 by volume). The graphene, P3HT, and PEDOT:PSS inks were printed with a 150 µm diameter nozzle. The flow rates of carrier gas and sheath gas, respectively, were 20 sccm and 70 sccm for graphene, 15 sccm and 30 sccm for P3HT, and 20 seem and 30 seem for PEDOT:PSS. Following printing, the TFTs were annealed at 160 °C for 30 min in air before electrical characterization.

Characterization

The exfoliated hBN nanoplatelets were observed using a scanning electron microscope (SU8030, Hitachi). Shear viscosity of the hBN ionogel ink was measured using a rheometer (MCR 302, Anton Paar) equipped with a 25 mm, 2° cone and plate geometry. Viscoelastic properties of the hBN ionogels were characterized using the rheometer equipped with a 25 mm diameter parallel plate

(gap between the rheometer stage and parallel plate: 1 mm) with a strain of 0.1%. Ionic conductivity (σ) of the hBN ionogels was calculated based on the following equation:

$$\sigma = \frac{t}{A \times R}$$

where t is the sample thickness, A is the sample area, and R is the bulk resistance determined by electrochemical impedance spectroscopy (VSP, BioLogic). Cross-sectional profiles of the printed hBN ionogels were obtained using a laser confocal microscope (OLS5000, OLYMPUS). Electrical performance of the fabricated TFTs was measured using source meters (2400, Keithley) in air at room temperature.

Conflicts of interest

The printable hBN ionogel ink is being commercialized in collaboration with MilliporeSigma.

Acknowledgements

We thank S. V. Rangnekar for her assistance in generating the aerosol jet printer patterning files. The printable hBN ionogel ink development was supported by MilliporeSigma and the U.S. Department of Commerce, National Institute of Standards and Technology (Award 70NANB19H005) as part of the Center for Hierarchical Materials Design (CHiMaD). Electrochemical characterization was supported by the Center for Electrochemical Energy Science, an Energy Frontier Research Center funded by the U.S. Department of Energy (DOE), Office of Science, Basic Energy Sciences under Award DE-AC02-06CH11357. Graphene powder processing was supported by the National Science Foundation Scalable Nanomanufacturing Program (NSF CMMI-1727846). SEM, TEM, and XPS were performed in the NUANCE facility at Northwestern University, which is supported by the Soft and Hybrid Nanotechnology Experimental (SHyNE) Resource (NSF ECCS-1542205), the Materials Research Science and Engineering Center (NSF DMR-1720139), the State of Illinois, and Northwestern University. Rheometry and thermogravimetric analysis were performed in the MatCI facility, which receives support from the NSF MRSEC Program (NSF DMR-1720139).

References

- A. C. Arias, S. E. Ready, R. Lujan, W. S. Wong, K. E. Paul, A. Salleo, M. L. Chabinyc, R. Apte and R. A. Street, *Appl. Phys. Lett.*, 2004, 85, 3304–3306.
- 2 M. Berggren, D. Nilsson and N. D. Robinson, Nat. Mater., 2007, 6, 3-5.
- 3 V. Subramanian, J. M. J. Fréchet, P. C. Chang, D. C. Huang, J. B. Lee, S. E. Molesa, A. R. Murphy, D. R. Redinger and S. K. Volkman, *Proc. IEEE*, 2005, 93, 1330–1338.
- 4 G. Mattana and D. Briand, Mater. Today, 2016, 19, 88-99.
- 5 K. Chen, W. Gao, S. Emaminejad, D. Kiriya, H. Ota, H. Y. Y. Nyein, K. Takei and A. Javey, *Adv. Mater.*, 2016, **28**, 4397–4414.
- 6 F. C. Krebs, Sol. Energy Mater. Sol. Cells, 2009, 93, 394-412.

- 7 S. Ito, P. Chen, P. Comte, M. Nazeeruddin, P. Liska, P. Pechy and M. Gratzel, *Prog. Photovoltaics*, 2007, **15**, 603–612.
- 8 L. J. Deiner and T. L. Reitz, Adv. Eng. Mater., 2017, 19, 1600878.
- 9 G. Chen, Y. Gu, H. Tsang, D. R. Hines and S. Das, Adv. Eng. Mater., 2018, 20, 1701084.
- 10 E. B. Secor, Flexible Printed Electron., 2018, 3, 035002.
- 11 K. Wang, Y.-H. Chang, C. Zhang and B. Wang, Carbon, 2016, 98, 397-403.
- 12 E. Jabari and E. Toyserkani, Mater. Lett., 2016, 174, 40-43.
- 13 B. A. Williams, A. Mahajan, M. A. Smeaton, C. S. Holgate, E. S. Aydil and L. F. Francis, ACS Appl. Mater. Interfaces, 2015, 7, 11526–11535.
- 14 E. Jabari and E. Toyserkani, Carbon, 2015, 91, 321-329.
- 15 L. Tu, S. Yuan, H. Zhang, P. Wang, X. Cui, J. Wang, Y.-Q. Zhan and L.-R. Zheng, J. Appl. Phys., 2018, 123, 174905.
- 16 J. G. Tait, E. Witkowska, M. Hirade, T.-H. Ke, P. E. Malinowski, S. Steudel, C. Adachi and P. Heremans, *Org. Electron.*, 2015, 22, 40–43.
- 17 L. J. Deiner, T. Jenkins, A. Powell, T. Howell and M. Rottmayer, *Adv. Eng. Mater.*, 2019, 21, 1801281.
- 18 J. H. Cho, J. Lee, Y. Xia, B. Kim, Y. He, M. J. Renn, T. P. Lodge and D. Frisbie, *Nat. Mater.*, 2008, 7, 900–906.
- 19 J. L. Bideau, L. Viau and A. Vioux, Chem. Soc. Rev., 2011, 40, 907-925.
- 20 S. Wang, B. Hsia, C. Carraroa and R. Maboudian, J. Mater. Chem. A, 2014, 2, 7997–8002.
- 21 N. Chen, H. Zhang, L. Li, R. Chen and S. Guo, Adv. Energy Mater., 2018, 8, 1702675.
- 22 Z. Jiadi, Y. Yuchao, J. Rundong, L. Zhongxin, Z. Wen, R. Z. Ur, B. Lin, Z. Xiaoxian, C. Yimao, S. Li and H. Ru, *Adv. Mater.*, 2018, 30, 1800195.
- 23 W. J. Hyun, A. C. M. de Moraes, J.-M. Lim, J. R. Downing, K.-Y. Park, M. T. Z. Tan and M. C. Hersam, ACS Nano, 2019, 13, 9664–9672.
- 24 Y. T. Liang and M. C. Hersam, J. Am. Chem. Soc., 2010, 132, 17661-17663.
- 25 A. C. M. de Moraes, W. J. Hyun, J.-W. T. Seo, J. R. Downing, J.-M. Lim and M. C. Hersam, Adv. Funct. Mater., 2019, 29, 1902245.
- 26 C. Cao, J. B. Andrews and A. D. Franklin, Adv. Electron. Mater., 2017, 3, 1700057.
- 27 C. Yang, E. Zhou, S. Miyanishi, K. Hashimoto and K. Tajima, ACS Appl. Mater. Interfaces, 2011, 3, 4053–4058.
- 28 K. Ueno, K. Hata, T. Katakabe, M. Kondoh and M. Watanabe, *J. Phys. Chem. B*, 2008, **112**, 9013–9019.
- 29 B. Avvaru, M. N. Patil, P. R. Gogate and A. B. Pandit, *Ultrasonics*, 2006, 44, 146–158.
- 30 K. Hayamizu, Y. Aihara, H. Nakagawa, T. Nukuda and W. S. Price, J. Phys. Chem. B, 2004, 108, 19527–19532.
- 31 A. Grandjean, M. Malki, C. Simonnet, D. Manara and B. Penelon, *Phys. Rev. B: Condens. Matter Mater. Phys.*, 2007, **75**, 054112.
- 32 Y. Lu, K. Korf, Y. Kambe, Z. Tu and L. A. Archer, *Angew. Chem., Int. Ed.*, 2014, 53, 488–492.
- 33 M. Patel, M. Gnanavel and A. J. Bhattacharyya, J. Mater. Chem., 2011, 21, 17419–17424.
- 34 Y. Lu, S. S. Moganty, J. L. Schaefer and L. A. Archer, J. Mater. Chem., 2012, 22, 4066–4072.

- 35 M. Ha, Y. Xia, A. A. Green, W. Zhang, M. J. Renn, C. H. Kim, M. C. Hersam and C. D. Frisbie, *ACS Nano*, 2010, 4, 4388–4395.
- 36 J.-H. Choi, W. Xie, Y. Gu, C. D. Frisbie and T. P. Lodge, *ACS Appl. Mater. Interfaces*, 2015, 7, 7294–7302.
- 37 K. Hong, S. H. Kim, K. H. Lee and C. D. Frisbie, *Adv. Mater.*, 2013, 25, 3413-3418.
- 38 B. Tang, S. P. White, C. D. Frisbie and T. P. Lodge, *Macromolecules*, 2015, 48, 4942–4950.
- 39 S. Ogawa, T. Naijo, Y. Kimura, H. Ishii and M. Niwano, Synth. Met., 2005, 153, 253–256.
- 40 S. H. Kim, K. Hong, W. Xie, K. H. Lee, S. Zhang, T. P. Lodge and C. D. Frisbie, Adv. Mater., 2013, 25, 1822–1846.
- 41 E. B. Secor, P. L. Prabhumirashi, K. Puntambekar, M. L. Geier and M. C. Hersam, *J. Phys. Chem. Lett.*, 2013, 4, 1347–1351.
- 42 E. B. Secor, B. Y. Ahn, T. Z. Gao, J. A. Lewis and M. C. Hersam, *Adv. Mater.*, 2015, 27, 6683–6688.